American Mineralogist, Volume 98, pages 2053–2062, 2013

Acoustic velocity measurements for stishovite across the post-stishovite phase transition under deviatoric stress: Implications for the seismic features of subducting slabs in the mid-mantle

Yuki Asahara[1,*], Kei Hirose[2,3], Yasuo Ohishi[4], Naohisa Hirao[4], Haruka Ozawa[3] and Motohiko Murakami[5]

[1]Earth and Space Science, Osaka University, Toyonaka 560-0043, Japan
[2]Earth-Life Science Instituite, Tokyo Institute of Technology, Meguro, Tokyo 152-8551, Japan
[3]Institute for Research on Earth Evolution, Japan Agency for Marine-Earth Science and Technology, Yokosuka, Kanagawa 237-0061, Japan
[4]Japan Synchrotron Radiation Research Institute (SPring-8), Sayo, Hyogo 679-5198, Japan
[5]Institute of Earth and Planetary Materials Science, Tohoku University, Sendai 980-8578, Japan

Abstract

Understanding effects of non-hydrostatic pressure on phase transitions in minerals relevant to the Earth's mantle is important to translate the observable seismic signals to not directly observable mineralogical models for the deep Earth. SiO_2 can occur as a free phase in subducting slabs, which contain sedimentary layers and/or mid-ocean-ridge basalts. In this study, we report on the effect of deviatoric strain on the pressure-induced phase transition in SiO_2 and its consequences on the seismic signal.

The acoustic velocity in polycrystalline stishovite across the post-stishovite phase transition was measured by Brillouin scattering in the pure SiO_2 system at room temperature under deviatoric stress. High-pressure synchrotron X-ray diffraction data were also collected at SPring-8. A linear fit to the symmetry-breaking strain values and the pressure of the transverse velocity minimum indicate a transition pressure between 25 and 35 GPa, which is about 20 GPa lower than that under hydrostatic conditions. The transverse velocity dropped by about 3% at around 25 GPa in this study. This is much smaller than the prediction from ab initio calculations that a transverse velocity reduces by ~60% at around 50 GPa under hydrostatic conditions. The results of the present study indicate that the deviatoric stress lowers the transition pressure and reduces the acoustic velocity change associated with the post stishovite phase transition. Sedimentary and mid ocean ridge basalt (MORB) layers in a subducting slab are likely sites for finding stishovite and its high-pressure polymorphs in the deep earth. Seismic observations of deep earthquakes occurring in subducting slabs indicate the existence of considerable stress in down-going slabs. This study suggests that nonhydrostatic deviatoric stress is one of the possible reasons for the absence of general seismic features that can be directly related to the post-stishovite phase transition in subducting slabs at 1500 km depth. The phase transition of stishovite under deviatoric stress, which occurs at shallower depths, can affect the local seismic scattering structures and the rheological behavior of a subducting slab in the mid-lower mantle region.

Keywords: High-pressure studies, stishovite, acoustic velocity, post-stishovite transition, deviatoric stress, subducting slab

Introduction

Silica (SiO_2) is one of the major constituents of the Earth's crust, and significant amounts of silica and silicates are transported to the deep earth by subducting slabs. Stishovite, a high-pressure polymorph of silica with Si in sixfold coordination, is considered to be an important constituent of subducted oceanic basalts and sediments in the Earth's deep interior. Stishovite exhibits the tetragonal rutile structure and transforms to the orthorhombic $CaCl_2$ structure above 50 GPa in the pure SiO_2 system (e.g., Tsuchida and Yagi 1989; Kingma et al. 1995; Andrault et al. 1998; Hemley et al. 2000; Andrault et al. 2003). This phase transition is being thought of as a classic displacive transition. According to theoretical models, the phase transition is triggered by the lattice instability of the soft transverse acoustic mode associated with the shear elastic constant; $(c_{11}-c_{12})/2$. A strong change in elastic properties is expected across the transition (e.g., Cohen 1992). Karki et al. (1997) reported that the shear wave velocity (v_S) decreases by 60% and the anisotropy increases by a factor of five prior to the transition from the tetragonal rutile structure to the orthorhombic $CaCl_2$ structure based on athermal first-principle calculations. They reported that the post-stishovite phase transition may cause discontinuous change in the shear wave velocity. Conversely, using a Landau free energy expansion, Carpenter et al. (2000) suggested that the variation in the transverse and longitudinal velocities might exhibit a dip instead of a discontinuity in the vicinity of the transitional pressure. For

* Present address: Institute of Earth and Planetary Materials Science, Tohoku University, Sendai 980-8578, Japan. E-mail: asahara.y@m.tohoku.ac.jp

0003-004X/13/1112–2053$05.00/DOI: http://dx.doi.org/10.2138/am.2013.4145

this considerable character across the transition, the nature of the post-stishovite phase transition has been the focus of much research in condensed-matter physics and Earth science.

The reported values for the transition pressure ranges widely from 40 to 90 GPa. This scatter results probably from the difficulty of identifying phase, the choice of pressure scales, as well as the effect of deviatoric stress. It is known that deviatoric stress affects the phase transformation pressures of crystals (e.g., Akaogi and Akimoto 1979). The effect of deviatoric stress is considered to be particularly strong for the post-stishovite phase transition. Dubrovinsky and Belonoshiko (1996), using molecular and lattice dynamics, suggested that deviatoric stress of about 1.5–2.5 GPa is sufficient to trigger the structural transformation to occur at much lower pressures than under hydrostatic conditions. Hemley et al. (2000) conducted high-pressure experiments using single-crystal stishovite in a hydrogen pressure medium and observed a hysteresis of transition; the transition between stishovite and the $CaCl_2$-structured phase occurred at 58 GPa along the compression path and at 40 GPa along the decompression path. The hysteresis of transition indicates a weak first-order character, and it may indicate a finite value of C_{11}-C_{12} at transition pressure. It is also possible that the hysteresis was a result of small deviatoric stress present in the sample. Andrault et al. (2003) conducted powder X-ray diffraction experiments for SiO_2 up to 130 GPa using the laser annealing technique and a NaCl pressure medium. They synthesized stishovite at around 12 GPa in the diamond-anvil cell and annealed the sample before conducting all measurements at 2300 K, where the stress relaxation was confirmed by the full-width at half maximum (FWHM) of the X-ray diffraction lines. They observed the transition pressure around 60 GPa. They also suggested that the post stishovite transition is essentially second-order based on strain and thermal energy analysis. Radial X-ray diffraction experiments and stress analyses across the post-stishovite phase transition under nonhydrostatic compression were conducted by Shieh et al. (2002). They used synthesized stishovite powder as a starting material and no pressure medium. The differential stress of stishovite was observed to be 4.5 GPa below 40 GPa, and was found to decrease in the pressure range between 40–50 GPa. They also observed that the difference between the volumes obtained across the maximum and minimum strain axes increased above 20 GPa. This indicates that lattice deformation of stishovite started around 20 GPa, although the differential stress in the sample reached a minimum around 50 GPa. From inversion of measured lattice strains, they suggested that elastic instability occurs in stishovite near 50 GPa.

The elastic constants of stishovite were measured at ambient conditions (Weidner et al. 1982; Brazhkin et al. 2005), and up to 12 GPa (Jiang et al. 2009) by Brillouin spectroscopy. However, there are no experimental acoustic velocity data for pure stishovite across the transition. Lakshtanov et al. (2007) conducted simultaneous Brillouin scattering and synchrotron X-ray diffraction measurements for hydrous alumina-bearing stishovite across the post-stishovite transition. The transition pressure for stishovite with impurities of 6 wt% Al_2O_3 and 0.24 wt% H_2O dropped to ~25 GPa. The acoustic shear velocity near the [110] phonon direction decreased by ~11%. In this phonon direction, the elastic shear modulus should vanish approaching the transition pressure, i.e., v_S becomes zero. The deviation from the [110] direction and the presence of impurities may be the reasons for the shear velocity not completely reaching zero at the transition pressure.

In this study, we measured acoustic velocities in pure, polycrystalline stishovite samples under nonhydrostatic conditions. In principle, acoustic velocity measurements under hydrostatic conditions should be performed to clarify the nature of the post-stishovite transition in the pure SiO_2 system. However, this is technically challenging and the experimental pressure has been limited to 12 GPa (Jiang et al. 2009). A method of measuring the acoustic velocities of stishovite and other lower-mantle phases under quasi-hydrostatic conditions at high temperatures and high pressures is required. With this in mind, we conducted acoustic velocity measurements of stishovite under nonhydrostatic conditions in the process of developing a method of quasi-hydrostatic measurements. Sedimentary and MORB layers in the subducting slab are plausible sites for high-pressure silica polymorphs to exist in the deep earth. Deep earthquakes reveal that subducting slabs are under considerable stress in the mantle. The present study may give insight on the seismic features and physical properties of subducting slabs.

Experimental methods

We synthesized a polycrystalline stishovite sample for Brillouin acoustic velocity and X-ray diffraction measurements by sintering SiO_2 reagent powder at 20 GPa and 1500 K using a Kawai-type multi-anvil apparatus. The sample was sufficiently transparent for Brillouin scattering. The synthesized pellet was analyzed using a scanning electron microprobe equipped with an electron dispersive spectrometer, and with an infrared spectrometer. The pellet consists of pure SiO_2 and has an OH concentration of ~20 ppm. X-ray diffraction was measured with a microfocused X-ray diffractmeter (Rigaku) with an anticathode of Cu; a wavelength of 1.5418 Å. The average grain size of the sintered pellet is about 1 μm. The pellet was double-side polished to a final thickness of about 40 μm, and cut with a diamond saw to about 80 μm square. The polycrystalline chip was loaded between thin NaCl pellets in a hole in a pre-indented rhenium gasket and confined in a symmetric diamond-anvil cell with a 60° angular aperture. Two beveled diamonds with 200 μm culets were used as anvils. A photograph of the sample is shown in Figure 1. The diameter of the sample chamber was about 100 μm. NaCl was used as the pressure medium and as a pressure gauge. The sample was compressed at 2–3 GPa intervals and was heated at 423 K in a vacuum oven to reduce the deviatoric stress in the sample chamber to below 10 GPa. Above 10 GPa, the compressed sample was heated using a CO_2 laser with an injected power of 20–30 W for about 60 s to reduce the deviatoric stress. We heated the sample to temperatures well below the condition at which irradiation started to prevent grain growth because the Brillouin signal is sensitive to crystallographic orientation (e.g., Shimizu et al. 1995; Baer et al. 1998). After heating, the pressure was measured using the Raman peak shift of diamond (Akahama and Kawamura 2006), and then the Brillouin scattering data were collected.

Brillouin scattering was performed with the system installed at SPring-8/BL10XU (Ohishi et al. 2008). A six-path tandem Fabry-Perot interferometer was used to collect the Brillouin spectra. A diode-pumped laser with a wavelength of 532 nm was used as the incident probe beam, and was focused on the sample to a spot size of ~20 μm in diameter. All measurements were performed in a symmetric scattering geometry with an external scattering angle (θ) of 49.0–50.7°, which was calibrated with a borosilicate crown optical glass (BK7; Yoneda and Song 2005) before measurements. Three separate series of experiments were conducted for the Brillouin scattering and X-ray diffraction measurements. The first series were performed along the compression path, and the second along both the compression and decompression paths. Two chips of polycrystalline stishovite were used for the first and second series, respectively. These were cut from the same sintered pellet. NaCl was used as a pressure medium. The collection of Brillouin scattering spectra was conducted at 1–65 GPa in the first and second series of experiments. The X-ray diffraction measurements were conducted at pressures of 1, 40, and ~60 GPa after the Brillouin scattering measurements on the same loading conditions, respectively.

The chip recovered from the second set of experiments was loaded with a small ruby sphere and a mixture of methanol-ethanol-water (in proportions of 16:3:1 by volume) for the third set of experiments to examine the effect of deviatoric stress on the sample during the high-pressure experiment. X-ray diffraction measurements were performed at pressure ranged 4.7–15.6 GPa along the compression path in the third series of experiments. We conducted Brillouin scattering measurements on the recovered sample only at 4.7 GPa. The recovered sample was partly deteriorated by the green laser injection, therefore, we did not measure Brillouin scattering of the sample at higher pressures.

We collected Brillouin spectra from three or four different positions and χ angles (χ angle: the angle rotated around the compression axis of the diamond-anvil cell) at fixed pressure conditions. The number of grains probed at a given pressure is about 1800–3200 estimated from the diameter of incident laser (20 μm) and the sample thickness (30–40 μm) under pressure, and number of measurements. We averaged the data at the same pressure conditions from the first and second series of experiments to ensure a representative average of acoustic velocity in the polycrystalline sample. The uncertainties of the individual velocity data were ±120 m/s (<1%) for v_P and ±80 m/s for v_S (<1.2%).

The X-ray diffraction measurements were conducted in four different experimental periods, and the experimental conditions and results are summarized in Table 1. The angle-dispersive X-ray diffraction spectra were collected using a CCD camera or an imaging plate. The incident X-ray beams were monochromized to wavelengths of 0.4130, 0.4135, 0.4136, and 0.4157 Å, respectively for each experimental period. The X-ray beam was collimated to 15 or 30 μm in diameter. The collection time for each X-ray diffraction measurement was about 120–240 s.

The pressure deviations of the different pressure scales, i.e., Raman frequency shift of the diamond and NaCl volume [Brown (1999) for B1 structure; Sakai et al. (2011) for B2 structure] and ruby fluorescence (Mao et al. 1978), were within ±3 GPa above the pressure of 15 GPa. This includes the uncertainty of the pressure determination and the pressure gradient in the sample chamber. The relationship between the pressures obtained with the diamond Raman scale and those obtained using the other scales are shown in Figure 2. Only the (110) diffraction from the B2-structured NaCl was observed. Therefore, we did not use B2-structured NaCl as a pressure scale but used this only as an indication showing the pressure gradient within the sample chamber. We used the B1-NaCl and the ruby scale below 20 GPa, and the diamond Raman scale above 20 GPa to determine the experimental pressure.

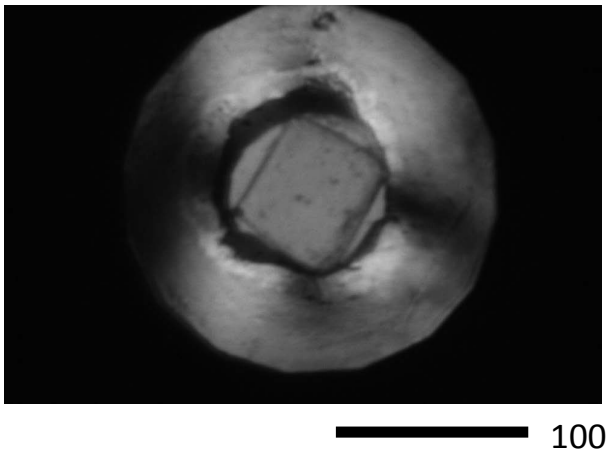

FIGURE 1. Photograph of a SiO_2 sintered pellet confined within the NaCl pressure medium in the diamond-anvil cell at 300 K and 40 GPa.

RESULTS

The circular two-dimensional X-ray diffraction pattern obtained in this study indicates that the sample was initially an isotropic aggregate with no preferred orientation (see supplementary figures[1]). The variations in measured acoustic velocity along χ angles were about 5.2% for longitudinal velocity (v_P) and 3.8% for transverse velocity (v_S) at 1 GPa (NaCl-B1 pressure gauge). These variations were <1.4% for v_P and <1.1% for v_S at higher pressures. There was no clear correlation between velocity

[1] Deposit item AM-13-1114, 2 supplemental figures. Deposit items are stored on the MSA web site and available via the American Mineralogist Table of Contents. Find the article in the table of contents at GSW (ammin.geoscienceworld.org) or MSA (www.minsocam.org), and then click on the deposit link.

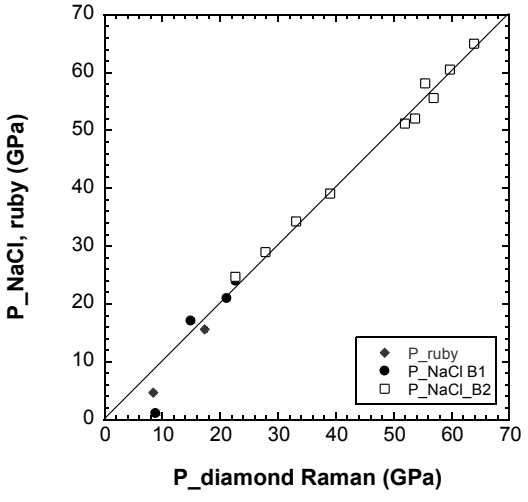

FIGURE 2. The relation between pressures obtained with the internal pressure scales of ruby and NaCl against the pressure obtained with the Raman edge frequency shift of a diamond culet.

TABLE 1. Experimental conditions and results for X-ray diffraction measurements

			SiO_2 rutile-type			SiO_2 $CaCl_2$-type			
	$P_{diamond\ Raman}$ (GPa)	$P_{NaCl\ B1}$ (GPa)	*a* (Å)	*c* (Å)	*V* (Å^3)	*a* (Å)	*b* (Å)	*c* (Å)	*V* (Å^3)
1		0.0001	4.174(1)	2.666(1)	46.45(2)				
				Compression					
2	8.8(7)*	1.10(2)	4.163(0)	2.660(0)	46.09(1)				
3	39(1)					4.049(2)	4.110(2)	2.611(1)	43.45(3)
4	56.9(1)					3.979(3)	4.097(3)	2.585(1)	42.14(5)
4	59.7(7)					3.963(4)	4.089(3)	2.575(2)	41.72(6)
4	63.9(7)					3.936(2)	4.086(2)	2.57(1)	41.33(3)
				Recovered sample compression					
		P_{ruby}							
5	8.4(1)*	4.7(3)	4.157(1)	2.658(0)	45.94(1)				
5		10.1(2)	4.133(1)	2.645(1)	45.18(2)				
5	17.3(3)	15.6(4)	4.115(1)	2.643(1)	44.75(3)				

Notes: The last digit of the error is in parentheses. Numbers in first column represent experimental series with wavelengths: 1 = 1.5418 Å; 2 = 0.4130(3) Å; 3 = 0.4136(2) Å; 4 = 0.4157(1) Å; 5 = 0.4135(1) Å.

* In the present study, the diamond Raman scale shows larger values than the pressures indicated by the NaCl-B1 pressure scale or the ruby scale below 10 GPa. This may be due to the fact that the diamond Raman scale by Akahama and Kawamura (2006) is mainly based on the data obtained above 20 GPa.

variation and χ angle. Relatively large variations in velocity at 1 GPa might indicate that the sample was not compacted well yet at that pressure. A representative Brillouin spectrum is shown in Figure 3. The longitudinal acoustic velocities and transverse acoustic velocities obtained as a function of pressure are shown in Figure 4. It is observed that the transverse velocity reaches a minimum between 20 and 30 GPa, whereas this is not observed for the longitudinal velocity. The v_P signal of stishovite always overlapped the v_S signal of single-crystal diamond, and therefore, the peak fitting has rather large uncertainties (<1%). The standard deviation of an average of measured velocities obtained from different series of experiments with NaCl pressure medium was <2% except for the value obtained at 20 GPa along the compression paths (2.7% for v_S). Measured velocities obtained during compression and decompression were comparable. It indicates that grain size reduction under pressure did not occur to a level that causes velocity reduction (Marquardt et al. 2011) in the present experiments. When a mixture of methanol-ethanol-water was used as a pressure medium, the measured velocity for the recovered sample was comparable with those obtained in the first and second series of experiments. The sample was deteriorated by the green laser at the first Brillouin scattering measurement, and therefore the Brillouin spectrum was collected only at 4.7 GPa for the third series of experiment.

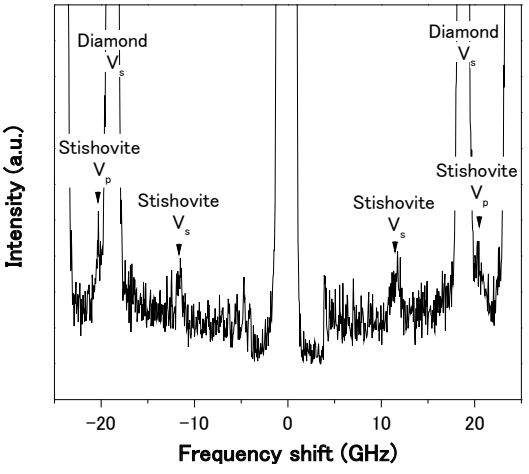

FIGURE 3. A representative Brillouin spectrum collected at 56 GPa and room temperature.

Representative integrated X-ray diffraction profiles collected at the pressures of 1, 16, 39, and 60 GPa are shown in Figure 5. The (211) of stishovite splits into two peaks above 30 GPa [i.e., (121) and (211) of the $CaCl_2$-structured phase], which indicates that the rutile-type structure is distorted to the $CaCl_2$-type structure (e.g., Andrault et al. 1998). A NaCl-B2 pressure gauge indicated that the pressure difference between the center and the edge of the stishovite pellet was about 2 GPa at 39 GPa. The broad FWHM in the X-ray diffraction profiles (Fig. 5) also indicate that a certain amount of stress remained after annealing.

It is known that the differentiation of the rutile-type structured phase and the $CaCl_2$-type structured phase is difficult with X-ray diffraction due to the similarity and small splitting. Therefore, we calculated the symmetry-breaking strain (Carpenter et al. 2000) to determine the transition pressure. The spontaneous strains e_1–e_3 for the tetragonal → orthorhombic transition are defined as $e_1 = (a–a_0)/a_0$, $e_2 = (b–a_0)/a_0$, and $e_3 = (c–c_0)/c_0$, where a, b, and c are the lattice parameters of the orthorhombic phase, and a_0 and c_0 are the lattice parameters of the tetragonal phase, extrapolated into the stability field of the orthorhombic phase [$a_0 = (a \times b)^{0.5}$]. The symmetry-breaking strain is $(e_1–e_2) = (a–b)/a_0$. The square of the measured symmetry-breaking strain is shown as a function of pressure in Figure 6 along with previous results (Andrault et al. 2003). The linear fit to the data, $(e_1–e_2)^2$ are greater than zero, and gives a transition pressure of 35 GPa. This transition pressure is considerably lower than the values reported in previous X-ray diffraction studies for single-crystal SiO_2 (stishovite) under quasi-hydrostatic conditions [50 GPa, Hemley et al. (2000)]; and for polycrystalline SiO_2 (stishovite) using the laser annealing method [60 GPa, Andrault et al. (2003)]. The unit-cell volume

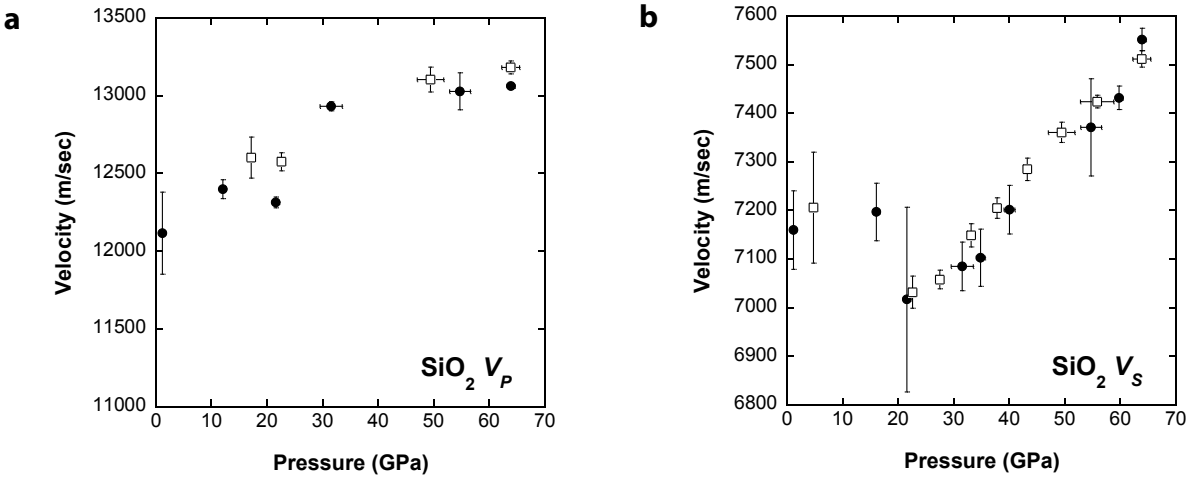

FIGURE 4. Acoustic velocities in polycrystalline stishovite measured in this study as a function of pressure: (**a**) longitudinal velocities and (**b**) transverse velocities. Filled circles and open squares represent acoustic velocities measured along compression and decompression paths, respectively. The uncertainties of the obtained velocity were calculated from uncertainty of peak fitting and standard deviation of averaged data.

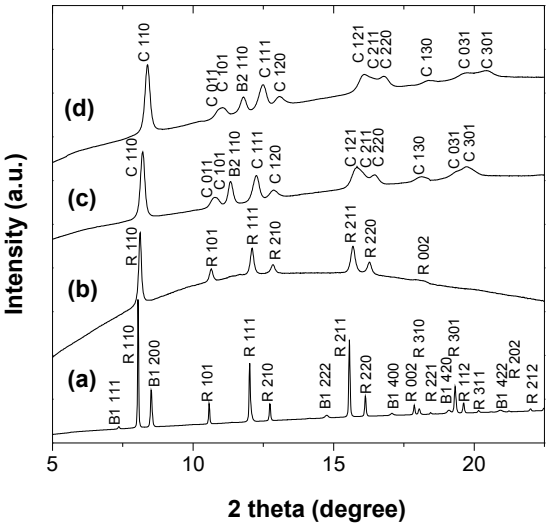

Figure 5. Representative integrated X-ray diffraction profiles of the sample (SiO_2 and NaCl) at room temperature and pressures of (**a**) 1 GPa, (**b**) 16 GPa, (**c**) 39 GPa, and (**d**) 60 GPa. Abbreviations of peaks are as follows: R, Rutile-type SiO_2; C, $CaCl_2$-type SiO_2; B1, B1-type NaCl.

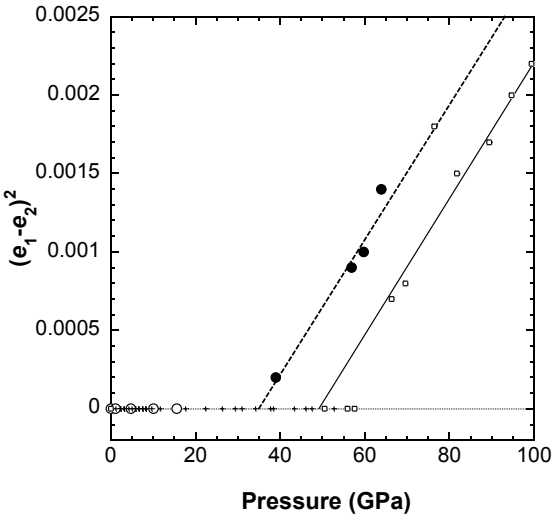

Figure 6. Square of the symmetry-breaking strain through the transition. Open and filled circles, the data obtained in this study for the rutile-structure phase and the $CaCl_2$-type phase, respectively; crosses and open squares, the data obtained by Andrault et al. (2003) for the rutile-structure phase and the $CaCl_2$-type phase, respectively. The bold dashed line and the solid line are a fit to the data for the $CaCl_2$-structured phase obtained in this study and Andrault et al. (2003), respectively; the thin dashed line is a horizontal line for zero.

and lattice parameters as a function of pressure determined in this study as well as in previous studies are shown in Figure 7. The unit-cell volume measured in this study deviated by ~3.2% over 30 GPa from the compression curve of stishovite, which was previously reported under hydrostatic conditions. This indicates that the nonhydrostatic effect became severer over 30 GPa. The compressibility of the **c**-axis measured in this study is almost comparable (within 0.3%) to that under hydrostatic conditions,

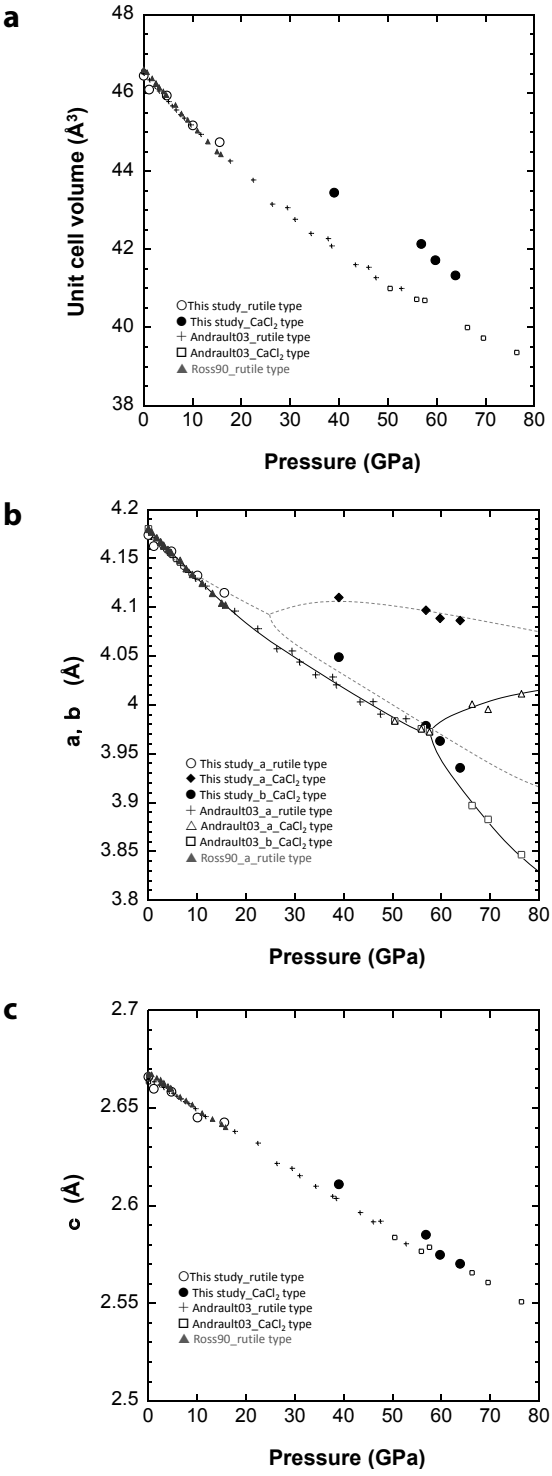

Figure 7. Volumes (**a**) and lattice parameters of SiO_2 phases as a function of pressure for *a* and *b* axes (**b**), and for *c* axes (**c**). Open circles: lattice parameters for the rutile-type phase obtained in this study; filled diamonds and filled circles: lattice parameters for the $CaCl_2$-type phase obtained in this study; crosses and gray filled triangles: lattice parameters for the rutile-type phase obtained by Andrault et al. (2003) and Ross et al. (1990), respectively. Open triangles and open squares: lattice parameters for the $CaCl_2$-type phase obtained by Andrault et al. (2003).

whereas the **a**-axis is less compressible than that under hydrostatic conditions. The linear fit to the symmetry-breaking strain and the transverse velocity minimum indicate that the transition pressure is in the range of 25–35 GPa in the present study.

We analyzed peak widths to obtain information about microstress with following procedure. Similar analyses have been conducted on energy dispersion X-ray profiles (e.g., Gerward et al. 1976; Weidner et al. 1998). Peak width broadened due to particle size, β_S, and distortions, β_D, in angle-dispersive diffraction are expressed through the following equations (Klug and Alexander 1974)

$$\beta_S(2\theta) = K\lambda / L\tan\theta \quad (1)$$

$$\beta_D(2\theta) = 4e\tan\theta \quad (2)$$

where K is the Scherrer constant, λ is the X-ray wavelength, θ is the scattering angle, L is the average crystalline size, and e is the approximate upper limit of strain.

With the assumptions as to the shape of the broadening profile due to crystallite size and strain, the observed widths, B, in the case of Lorentzian (Cauchy type) profiles is given by

$$B(2\theta) = \beta_S(2\theta) + \beta_D(2\theta). \quad (3)$$

The effect of a grain size of 1 μm, which was obtained by SEM analyses, is small and it is easily hidden in the instrumental contribution. If we apply Equation 1 (Scherrer equation) to estimate grain size of around 1 μm, we need a careful evaluation of instrumental broadening. Brillouin scattering results suggest that no apparent grain size reduction occurred in the present experiment. We therefore use this equation for the evaluation of instrumental contribution. Assuming that instrumental broadening can be included as a constant in the term of β_S and the crystallite size L is also constant in present study, then Equation 3 can be written as

$$B_S(2\theta) = (a\lambda/\cos\theta) + 4e\tan\theta \quad (4)$$

where a is a constant including the effects of instrumental contribution and crystallite size.

Figure 8 shows the observed peak widths given as full-width at half maximum (FWHM) of stishovite plotted against 2θ at 1.1 GPa obtained in this study. We obtained $a = 9.8 \times 10^6 \pm 0.8 \times 10^6$ m^{-1}, and an average upper limit of strain $e = 9.0 \times 10^{-4} \pm 0.7 \times 10^{-4}$ by fitting the FWHM data with Equation 4. We obtain upper limits of strain from independent peaks with the obtained value of a and Equation 4. Figures 9a and 9b show upper limits of strain from independent diffraction peaks plotted against d value and pressure, respectively. The uncertainty of the values is ~9%. Large deviation of the strain values from hkl = (101) compared to those from the other directions are the result of contamination of this reflection with the signal from (011) above 30 GPa. Except for the contaminated hkl = (101), the deviation between the strain values of hkl = (110) and (111) increases with increasing pressure above 30 GPa. The deviation may indicate that the deviatoric stress in the polycrystalline stishovite increases strongly with increasing pressure above 30

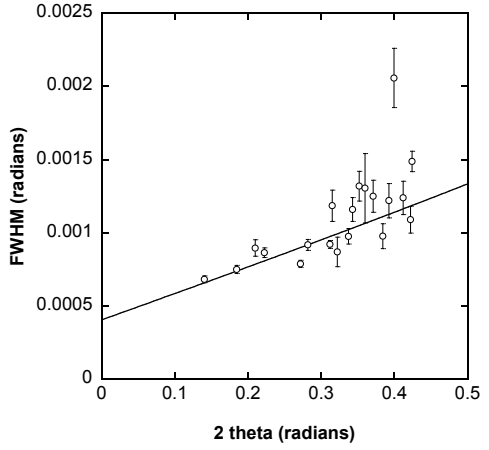

FIGURE 8. The FWHM of polycrystalline stishovite as a function of 2θ at 1 GPa. The curve shows weighted least-squares fit of Equation 4 to these data.

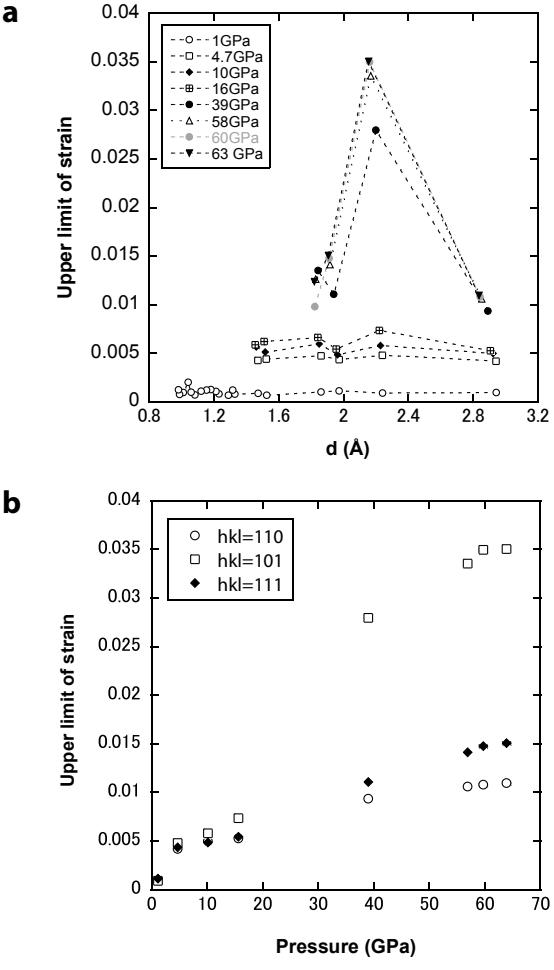

FIGURE 9. The approximate upper limit of strain obtained from the FWHM analysis (**a**) as a function of d value, (**b**) as a function of pressure. Relatively large values of upper limit of strain for hkl = (101) corresponding to the d-value of around 2.2 Å are due to contamination with the signal from hkl = (011) above 30 GPa.

GPa. To be exact, we need strain data and elastic constants for all independent orientation to obtain deviatoric stress. We report the values of the average upper limit of strain multiplied by the bulk modulus because this value indicates the stress range on the sample: The values are 2.3, 4.4, and 7.0 GPa at the experimental pressures of 16, 39, and 64 GPa, respectively. The bulk modulus of polycrystalline stishovite was obtained using acoustic velocity and density, which were measured in this study.

Figure 10 shows the acoustic velocity data for stishovite obtained in this and previous studies. The acoustic velocities of polycrystalline stishovite under nonhydrostatic conditions are comparable to the aggregate velocity obtained from the measured acoustic velocity of single-crystal stishovite under hydrostatic conditions by Jiang et al. (2009) and to predictions by Karki et al. (1997) and Carpenter et al. (2000) before the transition. The transverse velocity drop around 25 GPa in this study is about 3%, which is much smaller than the velocity reduction of 60% that is predicted under hydrostatic conditions at 50 GPa by ab initio calculations.

For a confirmation of the present result, we conducted a preliminary experiment using diamond anvils with 450 μm culets without X-ray diffraction measurements. The transverse velocity was measured with Brillouin scattering in a pressure range of 15–40 GPa. The transverse velocity minimum was observed at around 27 GPa with a 1.6% velocity reduction (see supplemental Fig. 2). The absolute values of the measured transverse velocity are ~100 m/s higher than those of the present experiments. This might be due to the difference of stress conditions and/or grain size in the sample.

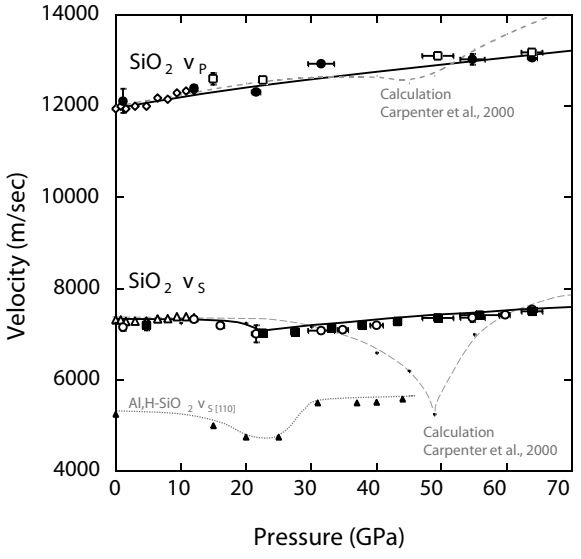

FIGURE 10. Acoustic velocities in SiO_2 phases as a function of pressure. Filled circles and open squares: longitudinal velocities measured in this study along compression and decompression paths, respectively; open circles and filled squares: transverse velocities measured in this study along compression and decompression paths, respectively; open diamonds and open triangles: longitudinal and transverse velocities for aggregate obtained from the measurement data for single-crystal SiO_2 by Jiang et al. (2009); solid triangles: acoustic velocities close to the [110] phonon direction of hydrous alumina bearing stishovite measured by Lakshtanov et al. (2007); gray dashed lines: aggregate velocity predicted by a Landau free energy calculation by Carpenter et al. (2000); solid lines: polynomial fit to the longitudinal velocities and transverse velocities measured in this study, respectively. Polynomial fits were made separately on transverse velocity at pressures below and above 25 GPa. The longitudinal velocities were not fitted separately because the data were not sufficient due to overlapping with diamond transverse velocity (see text): the gray dotted line is a visual guide for the measured velocities for Al- and H-bearing SiO_2.

DISCUSSION

A linear fit to the symmetry-breaking strain values and the pressure of the transverse velocity minimum indicates a transition pressure between 25 and 35 GPa in the present study. This transition pressure is considerably lower than the values that were reported in previous X-ray diffraction studies for single-crystal SiO_2 (stishovite) under quasi-hydrostatic conditions (Hemley et al. 2000) and for polycrystalline SiO_2 (stishovite) using the laser annealing method (Andrault et al. 2003). The lower transition pressure observed in the present study might be caused by relatively large deviatoric stress in the sample, although the laser annealing method used in the present study was similar to that of Andrault et al. (2003). A stress condition is estimated as a pivotal pressure gradient (2 GPa/50 μm at 39 GPa with a NaCl-B2 pressure gauge) in the present study. The estimated pressure gradient is a lower bound due to the low-shear strength of NaCl. The high-shear strength of SiO_2 may allow higher shear stress to be stored than that inferred from NaCl. Sintered polycrystalline stishovite, which was synthesized and recovered from a high-pressure and high-temperature experiment, was used as a starting material in the present study, whereas in situ synthesized stishovite was used in Andrault et al. (2003). It is plausible that the difference in sample preparation methods caused the difference in stress distribution in the sample because of the high-shear strength of stishovite. Furthermore, Andrault et al. (2003) conducted laser annealing at 2300 K to attain almost hydrostatic conditions, whereas, in the present study, laser annealing was conducted below the temperature threshold at which irradiation started, to prevent grain growth. The post-stishovite transition is known to be strongly affected by a deviatoric stress (e.g., Tsuchida and Yagi 1989), and the high-shear strength of stishovite causes large deviatoric stresses under nonhydrostatic conditions (e.g., Hemley et al. 2000). Dubrovinsky and Belonoshiko (1996) showed that even small deviatoric stress could affect the post-stishovite phase transition. The method of identification of transitional pressure in the present study was the same as that in Andrault et al. (2003). Therefore, the difference in a stress condition is likely to be one of the main sources for the lower transition pressure obtained in this study.

The results of this study are also inconsistent with the results of a radial X-ray diffraction experiment conducted under nonhydrostatic conditions by Shieh et al. (2002). They reported that the differential strain in the sample was around 4.5 GPa below 40 GPa and decreased to a minimum at around 48 GPa. Therefore, the displacive transition occurred at ~48 GPa, although the volume began to deviate from the values under nonhydrostatic conditions at around 20 GPa in the case of Shieh et al. (2002). We consider that the differences between the present study and that by Shieh et al. (2002) resulted from different stress distri-

butions in the samples. This is plausible, because Shieh et al. (2002) used synthesized powder without a pressure medium and did not conduct laser annealing, whereas the present study used a sintered pellet with a NaCl pressure medium and moderate laser annealing. Volume differences between the values obtained under hydrostatic conditions and under deviatoric stress were ~3% in the present study, and ~2% in Shieh et al. (2002). It may imply that deviatoric stress conditions in the present study is relatively larger than the value of 4.5 GPa observed in the experiment by Shieh et al. (2002). Acoustic velocity measurements under controlled stress conditions with dense X-ray diffraction data, hopefully with a radial X-ray diffraction method, should be conducted to examine this inference.

If the observed velocity minima at around 22 GPa marks the beginning of the transition, it takes about 18 GPa for the $CaCl_2$ phase to reach a transverse velocity value comparable to the one of the stishovite before softening. This pressure range is much larger than that reported by previous studies; 0 GPa was reported with ab initio calculation for pure SiO_2 by Karki et al. (1997), around 5 GPa for experimental observation on hydrous alumina bearing SiO_2 by Lakshtanov et al. (2007), and around 11 GPa suggested using a Landau free energy expansion for pure SiO_2 by Carpenter et al. (2000). In the present study, the acoustic velocity of polycrystalline SiO_2 was measured. Therefore, the obtained velocity is an average of each SiO_2 grain. The small velocity drop observed in the present study may indicate that the phase transition was gradual and corresponds to the heterogeneous stress distribution at intergranular contacts in the sample; as a result, the strong elastic softening feature of post-stishovite transition was suppressed. The relatively large pressure interval of velocity rebound might also be a result of the overlapping of velocity minima in individual grains. Partial dislocations associated with the shear induced phase transition may also affect the reduction of velocity change across the transition (e.g., Putonis 1992). There is no clear difference between data measured along compression path and decompression path in the present result. Consistent absolute values might imply that the grain size in the sample did not change noticeably during compression. However, the hysteresis of transition pressure might exist at least for the difference of stress condition between compression path and decompression path. When we examine the data on compression and decompression separately, compression data indicate that velocity minima may exist between 20 and 30 GPa and decompression data indicates velocity minima may exist between 10 and 20 GPa. In the present study, the deviatoric stress seems to suppress clear transition features of the post stishovite phase transition. To better discuss the hysteresis and the change of elastic properties accompanying the post-stishovite phase transition, hydrostatic experiments should be conducted with dense X-ray diffraction and acoustic velocity measurements.

It is predicted that even a few volume percent of free silica can provide observable seismic reflections in the mid-lower mantle because of the anomalous reduction in shear velocity associated with the post-stishovite phase transition (Karki et al. 1997). A basaltic layer in the subducting slab contains about 10–25 vol% of free SiO_2 in the deep mantle region (e.g., Ono et al. 2001). Therefore, a seismic anomaly could be observed as a general feature where subducting or upwelling oceanic crust exists. In fact, there are several seismic reflectors at 800–1800 km depth, which may be related to the post-stishovite phase transition (Kawakatsu and Niu 1994; Le Stunff et al. 1995; Kaneshima and Helffrich 1999, 2010; Vinnik et al. 2001; Niu et al. 2003; Kaneshima 2009; Vinnik et al. 2010). Several individual groups have investigated the phase boundary between stishovite and the $CaCl_2$-structured phase at high temperature, and the results are rather controversial due to difficulties in phase determination and choice of pressure scales, and the effect of deviatoric stress (e.g., Kingma et al. 1995; Ono et al. 2002; Tsuchiya et al. 2004; Nomura et al. 2010). Most recently, Nomura et al. (2010) determined the phase boundary at temperatures of 300–2500 K using a laser-heated diamond-anvil cell experiment. They determined the phase boundary to be at 50 GPa at 300 K with a positive Clapeyron slope of 11.1 MPa/K. The transitional pressure in the pure SiO_2 system was found at 56–70 GPa for typical slab and mantle geotherms, which corresponds to the reflectors at a depth of around 1500 km (Kaneshima and Helffrich 1999, 2010) in the mantle and is still higher than the pressure corresponding to the reflectors at 800–1200 km depth. The effect of impurities such as Al and H in the SiO_2 phases is one of the possible explanations for the seismic reflectors at 800–1200 km depth (Lakshtanov et al. 2007), but this explanation does not exclude other possibilities such as compositional layering or decomposition of phase D (e.g., Kawakatsu and Niu 1994). A reduction in shear velocity across the post-stishovite transition as a result of Al or H impurities in stishovite is about 11% at a direction near [110] (Lakshtanov et al. 2007). The transition might be visible in seismic profiles if a subducting slab is under hydrostatic conditions. However, seismic observations indicating the occurrence of the post-stishovite transition accompanied with strong v_S reductions have only been observed locally, despite the large influence expected (Kaneshima and Helffrich 2010). Experimental investigation of the acoustic velocity in stishovite under hydrostatic conditions at high temperatures and pressures should be undertaken to clarify the nature of the post-stishovite phase transition. However, the present results may suggest that nonhydrostaticity in the subducting slab is one of the possible reasons for the absence of general seismic features in the subducting slabs that clearly relate to the post-stishovite phase transition accompanied by extremely low-shear velocity anomalies. The present study reveals that nonhydrostatic deviatoric stress reduces the transitional pressure and velocity change. Therefore, if the post-stishovite phase transition occurs at lower pressures under nonhydrostatic stress, the phase transition of stishovite containing some or no impurities does not occur at transitional pressures with expected velocity reductions under hydrostatic conditions in the downgoing slab. Silica-bearing layers such as basalts and sediments are likely to be stretched and folded in the mid-lower mantle; therefore, a velocity change of <3% due to the phase transition of stishovite might be obscured by anomalies caused by temperature differences or chemical and structural heterogeneity. However, this phase transition of stishovite under deviatoric stress could affect the generation of scattering objects in the mid-lower mantle (e.g., Kaneshima and Helffrich 2010) and also could influence the rheological behavior of a subducting slab, such as slab thickening observed in the mid-lower mantle (Van der Hilst 1995; Shellart et al. 2009; Zhao 2004).

The deviatoric stress in the present study was estimated to be 2 GPa from the pressure distribution in the sample obtained using the NaCl-B2 pressure gauge. However, the difference between the volumes of stishovite obtained in this study and in previous studies under hydrostatic conditions and under deviatoric stress implies that stress conditions in stishovite were larger than a value of about 4.5 GPa. This is in the possible stress range for a subducting slab based on the stress capacity of major constituent minerals (Chen 2010), although the actual stress conditions in the subducting slab are not known. According to the stress measurements for mantle phases (e.g., Weidner et al. 1998; Chen 2010), differential stress decreases with increasing temperature. Weidner et al. (1998) demonstrated that microstrain in stishovite decreased to 20% of the initial strain with increasing temperature up to 1273 K at experimental pressure of 12 GPa. The experimental condition is close to the coesite-stishovite phase boundary (Akaogi et al. 1995). Stishovite has a wide stability field from 8 to 60 GPa along the cold slab geotherms (e.g., Kirby et al. 1996) that corresponds to the range from the transition zone to the mid-lower mantle region of the Earth, The stress capacity of stishovite under higher pressures is still unclear. Although the value depends on the mineral phases, the rate of reduction was estimated to be 60 and 20% at 20 GPa and 1073 K for ringwoodite and perovskite, respectively (Chen 2010). This implies that the stress capacity of minerals is small under mid-lower mantle conditions. In the mid-lower mantle region, the stress conditions might be weaker than that in the region shallower than 700 km depth because of stress-reducing processes such as seismic energy release and recrystallization annealing across the perovskite-forming reaction (e.g., Bina 2010). However, it is plausible that a certain deviatoric stress exists in silica-rich layers even in the mid-lower mantle region, as a result of the high-shear strength of stishovite. The results presented here suggest the possibility that the post-stishovite phase transition under deviatoric stress explains the lack of general seismic features of extreme reductions in shear velocity related to the post stishovite transition in the mid-lower mantle. The post-stishovite transition that occurs at lower pressures under nonhydrostatic conditions may affect the local seismic scattering structures and the rheological behavior of subducting slabs, as displayed by slab-thickening features observed in the mid-mantle region. The effect of stress on the transitional pressure and the elasticity change of stishovite at high temperatures should be investigated with accurate stress estimation for further discussion.

ACKNOWLEDGMENTS

We thank K. Funakoshi, Y. Higo, and T. Matsuzaki for their help in sample preparation, and K. Kudo, L. Dai, and T. Tsuchiya for valuable discussions. We also thank K. Nagaki and K. Tanaka for their help in microprobe analysis. T. Sakai and A. Suzuki are appreciated for their help in FT-IR measurement. We appreciate C. Bina and two anonymous reviewers for constructive suggestions. T. Kondo and E. Ohtani are appreciated for their fundamental support. Y.A. was partially supported by a JSPS research fellowship for young scientists. This study was performed under the approval of the following proposal numbers: 2009B0087, 2010A0087, 2010B0087, and 2011A1440 of SPring-8. This study was partially carried out under the Visiting Researcher's Program of the Institute for Study of the Earth's Interior, Okayama University. The authors thank Enago (www.enago.jp) for the English language review.

REFERENCES CITED

Akahama, Y., and Kawamura, H. (2006) Pressure calibration of diamond anvil Raman gauge to 310 GPa. Journal of Applied Physics, 100, 043516.

Akaogi, M., and Akimoto, S. (1979) High pressure phase equilibria in a garnet lherzolite, with special reference to Mg^{2+}-Fe^{2+} partitioning among constituent minerals. Physics and the Earth and Planetary Interiors, 19, 31–51.

Akaogi, M., Yusa, H., Shiraishi, K., and Suzuki, T. (1995) Thermodynamic properties of α-quartz, coesite, and stishovite and equilibrium phase relations at high pressures and high temperatures. Journal of Geophysical Reserch, 100, 22337–22347.

Andrault, D., Fiquet, G., Guyot, F., and Hanfland, M. (1998) Pressure-induced Landau-type transition in stishovite. Science, 282, 720–724.

Andrault, D., Angel, R.J., Mosenfelder, J.L., and Le Bihan, T. (2003) Equation of state of stishovite to lower mantle pressures. American Mineralogist, 88, 301–307.

Baer, B.J., Brown, J.M., Zaug, J.M., Schiferl, D., and Chronister, E. (1998) Impulsive stimulated scattering in ice VI and ice VII. Journal of Chemical Physics, 108, 4540–4544.

Bina, C.R. (2010) Scale limits of free-silica seismic scatters in the lower mantle. Physics of the Earth and Planetary Interiors, 183, 110–114.

Brazhkin, V.V., McNeil, L.E., Grimsditch, L.E., Bendeliani, N.A., Dyuzheva, T.I., and Lityagina, L.M. (2005) Elastic constants of stishovite up to its amorphization temperature. Journal of Physics: Condensed Matter, 17, 1869–1875.

Brown, J.M. (1999) The NaCl pressure standard. Journal of Applied Physics, 86, 5801–5808.

Carpenter, M., Hemley, M.A., and Mao, H.K. (2000) High-pressure elasticity of stishovite and the P42/mnm-Pnnm phase transition. Journal of Geophysical Research, 105, 10807–10816.

Chen, J. (2010) Understanding depth variation of deep seismicity from in situ measurements of mineral strength at high pressures. Journal of Physics and Chemistry of Solids, 71, 1032–1037.

Cohen, R.E. (1992) First-principles predictions of elasticity and phase transitions in high pressure SiO_2 and geophysical implications. In Y. Syono and M.H. Manghnani, Eds., High Pressure Research: Application to Earth and Planetary sciences, 425 p. American Geophysical Union, Washington, D.C.

Dubrovinsky, L.S., and Belonoshiko, A.B. (1996) Pressure-induced phase transition and structural changes under deviatoric stress of stishovite to $CaCl_2$-like structure. Geochimica et Cosmochimica Acta, 60, 3657–3663.

Gerward, L., Mørup, S., and Topsøe, H. (1976) Particle size and strain broadening in energy-dispersive X-ray powder patterns. Journal of Applied Physics, 47, 822–825.

Hemley, R.J., Shu, J., Carpenter, M.A., Hu, J., Mao, H.K., and Kingma, K.J. (2000) Strain/order parameter coupling in the ferroelastic transition in dense SiO_2. Solid State Communications, 114, 527–532.

Jiang, F., Gwanmesia, G.D., Dyuzheva, T.D., and Duffy, T.S. (2009) Elasticity of stishovite and acoustic mode softening under high pressure by Brillouin scattering. Physics of the Earth and Planetary Interiors, 172. 235–240.

Kaneshima, S. (2009) Seismic scatterers at the shallowest lower mantle beneath subducted slabs. Earth and Planetary Science Letters, 286, 304–315.

Kaneshima, S., and Helffrich, G. (1999) Dipping low-velocity layer in the mid-lower mantle: Evidence for geochemical heterogeneity. Science, 283, 1888–1891.

——— (2010) Small scale heterogeneity in the mid-lower mantle beneath the circum-Pacific area. Physics of the Earth and Planetary Interiors, 183, 91–103.

Karki, B.B., Stixrude, L., and Crain, J. (1997) Ab initio elasticity of three high-pressure polymorphs of silica. Geophysical Research Letters, 24. 3269–3272.

Kawakatsu, H., and Niu, F.L. (1994) Seismic evidence for a 920 km discontinuity in the mantle. Nature, 371, 301–305.

Kingma, K.J., Cohen, R.E., Hemley, R.J., and Mao, H.K. (1995) Transformation of stishovite to a denser phase at lower-mantle pressures. Nature, 374, 243–245.

Kirby, S.H., Stein, S., Okal, E.A., and Rubie, D.C. (1996) Metastable mantle phase transformations and deep earthquakes in subducting oceanic lithosphere. Reviews of Geophysics, 34, 261–306.

Klug, H.P., and Alexander, H.P. (1974) Crystallite size and lattice strains from line broadening. In X-ray Diffraction Procedures, 2nd ed., 618–708. Wiley, New York.

Lakshtanov, D.L., Sinogeikin, S.V., Litasov, K.D., Prakapenka, V.B., Hellwig, H., Wang, J., Sanches-Valle, C., Perrillat, J.P., Chen, B., Somayazulu, M., and others. (2007) The post-stishovite phase transition in hydrous alumina-bearing SiO_2 in the lower mantle of the earth. Proceedings of the National Academy of Science, 104, 13588–13590.

Le Stunff, Y., Wicks, C.W. Jr., and Romanowicsz, B. (1995) P′P′ precursors under Africa: Evidence for mid-mantle reflectors. Science, 270, 74–77.

Mao, H.K., Bell, P.M., Shaner, W.G., and Steinberg, D.J. (1978) Specific volume measurements of Cu, Mo, Pd, and Ag and calibration of the ruby R1 fluorescence pressure gauge from 0.06 to 1 Mbar. Journal of Applied Physics, 49, 3276–3283.

Marquardt, H., Gleason, A., Marquardt, K., Speziale, S., Miyagi, L., Neusser, G., Wenk, H.-R., and Jeanloz, R. (2011) Elastic properties of MgO nanocrystals and grain boundaries at high pressures by Brillouin scattering. Physical Review B, 84, 064131.

Niu, F., Kawakatsu, H., and Fukao, Y. (2003) Seismic evidence for a chemical heterogeneity in the midmantle: A strong and slightly dipping seismic reflector beneath the Mariana subduction zone. Journal of Geophysical Research,

108(B9), 2419, doi:10.1029/2002JB002384.
Nomura, R., Hirose, K., Sata, N., and Ohishi, Y. (2010) Precise determination of post-stishovite phase transition boundary and implications for seismic heterogeneities in the mid-lower mantle. Physics of the Earth and Planetary Interiors, 183, 104–109.
Ohishi, Y., Hirao, N., Sata, N., Hirose, K., and Takata, M. (2008) Highly intense monochromatic X-ray diffraction facility for high-pressure research at SPring-8. High Pressure Research, 28, 163–173.
Ono, S., Ito, E., and Kastura, T. (2001) Mineralogy of subducted basaltic crust (MORB) from 25 to 37 GPa, and chemical heterogeneity of the lower mantle. Earth and Planetary Science Letters, 190, 57–63.
Ono, S., Hirose, K., Murakami, M., and Isshiki, M. (2002) Post-stishovite phase boundary in SiO_2 determined by in situ X-ray observations. Earth and Planetary Science Letters, 197, 187–192.
Putonis, A. (1992) Twin boundaries. In Introduction to Mineral Sciences, 223–234. Cambridge University Press, U.K.
Ross, N.L., Shu, J.F., Hazen, R.M., and Gasparik, T. (1990) High pressure crystal chemistry of stishovite. American Mineralogist, 75, 739–747.
Sakai, T., Ohtani, E., Hirao, N., and Ohishi, Y. (2011) Equation of state of the NaCl-B2 phase up to 304 GPa. Journal of Applied Physics, 109, 084912.
Shellart, W.P., Freeman, J., Stegman, D.R., Moresui, L., and May, D. (2009) Evolution and diversity of subduction zones controlled by slab width. Nature, 446, 308–311.
Shieh, S.R., T.S. Duffy, and Li, B. (2002) Strength and elasticity of SiO_2 across the stishovite–$CaCl_2$-type structural phase boundary. Physical Review Letters, 89, 255507.
Shimizu, H., Ohnishi, M., and Sasaki, S. (1995) Cauchy relation in dense H_2O ice VII. Physical Review Letters, 74, 2820–2823.
Tsuchida, Y., and Yagi, T. (1989) A new, post stishovite high-pressure polymorph of silica. Nature, 340, 217–220.
Tsuchiya, T., Caracas, R., and Tsuchiya, J. (2004) First principles determination of the phase boundaries of high-pressure polymorphs of silica. Geophysical Research Letters, 31, L11610, doi: 10.1029/2004GL019649.
Van der Hilst, R. (1995) Complex morphology of subducted lithosphere in the mantle benearth the Tonga trench. Nature, 374, 154–157.
Vinnik, L., Kato, M., and Kawakatsu, H. (2001) Search for seismic discontinuities in the lower mantle. Geophysical Journal International, 147, 41–56.
Vinnik, L.P., Oreshin, S.I., Speziale, S., and Weber, M. (2010) Mid-mantle layering from SKS receiver functions. Geophysical Research Letters, 37, L24302.
Weidner, D.J., Bass, J.D., Ringwood, A.E., and Sinclair, W. (1982) The single-crystal elastic moduli of stishovite. Journal of Geophysical Research, 87, 4740–4746.
Weidner, D.J., Wang, Y., Chen, G., Ando, J., and Vaughan, M.T. (1998) Rheology measurement at high pressure and temperature. In M.H. Manghnani, and T. Yagi, Eds., Properties of Earth and Planetary Materials at Pressure and Temperature, 101, 473–482. Gephysical Monograph, American Geophysical Union, Washington, D.C.
Yoneda, A., and Song, M. (2005) Frequency domain analysis of ultrasonic velocity: An alternative bond effect correction constraining bond properties. Journal of Applied Physics, 97, 024908.
Zhao, D. (2004) Global tomographic images of mantle plumes and subducting slabs: Insight into deep earth dynamics. Physics of Earth and Planetary Interiors, 146, 3–34.

Manuscript received February 25, 2012
Manuscript accepted July 17, 2013
Manuscript handled by Jennifer Kung